

Breakdown of Quasilinear Theory in the Tokamak Edge

Arash Ashourvan^{*} and J. Candy[†]
General Atomics, San Diego, California, USA

 (Received 12 December 2023; accepted 11 April 2024; published 13 May 2024)

In the edge of an L -mode tokamak plasma, particle transport and ion energy transport are shown to follow a strong microturbulence (SMT) scaling, whereas in the plasma core the transport is shown to follow quasilinear turbulence scaling. The dependence of diffusivity on potential fluctuation amplitude is linear in the SMT regime, and quadratic in the quasilinear regime. The transition to strong microturbulence results from larger $E \times B$ drift velocities in the edge compared to the plasma core. At these larger velocities, ions traverse the spatially correlated range faster than the stochastic evolution of the electric potential. Hence, these particles do not experience a time-stochastic field as required by the quasilinear approximation. Instead, scattering of particles in the SMT regime is caused by spatial stochasticity. In contrast, electron energy transport remains quasilinear due to decorrelations caused by collisions and fast parallel motion. Improved understanding of transport beyond quasilinear theory opens the path to more accurate modeling of transport in the tokamak plasma edge.

DOI: [10.1103/PhysRevLett.132.205101](https://doi.org/10.1103/PhysRevLett.132.205101)

Introduction.—Following years of dedicated experimental campaigns in tokamaks, and employing high-fidelity gyrokinetic (GK) simulations and transport modeling, understanding of key aspects of the turbulence and transport in the core of the tokamak plasma is relatively mature. Naturally, the radial edge of plasma, for which $r/a \gtrsim 0.9$ (where a is the plasma minor radius), emerges as the next frontier for improved physics understanding and modeling fidelity. This redirection of focus to the plasma edge has been out of necessity: the plasma edge serves as the boundary condition to the plasma core, and any prediction of the fusion performance of plasma will demand an accurate representation of the edge. One such challenge for predictive modeling has been the calculation of the power threshold required for the transition from the low-confinement mode (L mode) to high-confinement mode (H mode) [1,2]. The latter, identified by the formation of a pedestal in the outer edge of the radial temperature and density plasma profiles, is the high performance operational regime intended for all future tokamaks. Prediction of the L - H transition power threshold will naturally require a thorough understanding of the nature of turbulent transport and saturation mechanisms in the edge of L -mode pedestal.

While GK simulations, serving as interpretive tools, have significantly advanced our understanding of turbulence and transport, effectively the only tools for predictive modeling of transport so far have been based on the quasilinear (QL) approximation [3–7], which is the simplest practical theory of plasma turbulence. In essence, QL theory is a mean-field, perturbation approximation for weak turbulence, and the equations solved are first order and linear in gyrokinetic ordering parameter $\varepsilon \sim \delta f/F \sim e\delta\phi/T_e \sim \rho_s/L \ll 1$, where δf and F are the fluctuating and the equilibrium part of the

distribution function, $\delta\phi$ is the electric potential fluctuation, T_e is the electron temperature, $\rho_s = c_s/\Omega_{ci}$ is the ion sound gyroradius, and L is a characteristic macroscopic radial length scale; $c_s = \sqrt{T_e/m_i}$ is the ion sound speed, m_i is ion mass, and Ω_{ci} is the ion cyclotron frequency. The transport fluxes calculated by QL models have a quadratic dependence on the amplitude of the saturated potential $\delta\phi$. The amplitude is predicted using saturation rules that are typically based on mixing length theory [8]. Further, physical effects critical to turbulent transport have also been modeled and included in QL-based transport calculations ($E \times B$ shear [9,10], zonal-flow mixing [11], geometry effects [12], rotation and temperature anisotropy induced poloidal asymmetry [13]). Finally, using a number of free parameters, the QL model is calibrated to a database of nonlinear (NL) gyrokinetic simulations [12,14], or also using experimental observations [15]. Breakdown of a QL model was observed in Ref. [16] for the ion energy flux in comparison to the flux calculated by GYRO [17] for the ion-temperature gradient turbulence with adiabatic electrons. Departure between a QL model (QuaLiKiz) [15] and a flux driven, full f-GK code (GYSELA) [18] has also been observed [19], although the physics of that departure is beyond the scope of the gradient-driven, δf -GK formalism employed in this Letter.

In this Letter we examine the validity of QL theory, and show that this validity is broken for deuterium ions in the edge of an L -mode plasma. In essence, breakdown of QL approximation in the edge is the result of larger particle $E \times B$ drift velocities in stronger turbulence fields. These particles traverse their spatially correlated range [20] before the stochastic evolution of the electric potential which

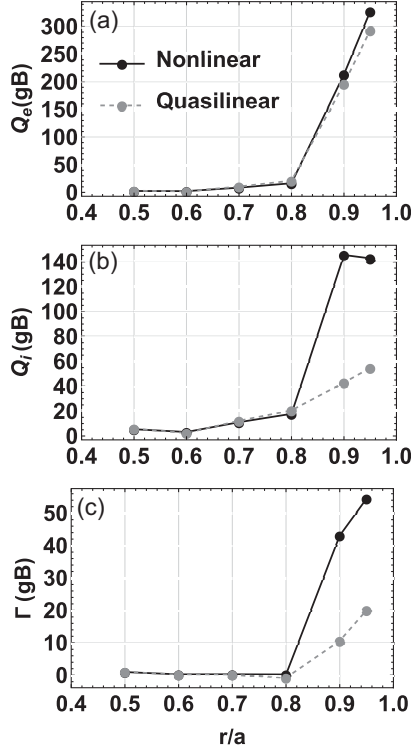


FIG. 1. Nonlinear fluxes of (a) electron energy Q_e , (b) ion energy Q_i , and (c) particles Γ in gyroBohm units (gB) calculated with CGYRO (black) versus quasilinear fluxes (gray) calculated from Eqs. (1) and (2).

consists of an intricate landscape of irregularly spaced wells and hills. In contrast, the validity of QL theory requires that the potential landscape should evolve before particles leave one spatially correlated turbulence region for another [21]. We further show that for electrons the combined effects of parallel motion and collisional decorrelation lead to quasilinear turbulence scaling (QLT scaling) of transport, even when ion transport scaling is clearly not QLT.

Comparison of NL and QL transport.—Fluxes calculated by a QL model for turbulent transport have the form [12]

$$Q_a^{\text{QL}} = c_{\text{free}} \Delta K_y \sum_{k_y} W Q_{k_y}^a |\Phi_{k_y}(\theta=0)|^2, \quad a = i, e \quad (1)$$

$$\Gamma^{\text{QL}} = c_{\text{free}} \Delta K_y \sum_{k_y} W \Gamma_{k_y} |\Phi_{k_y}(\theta=0)|^2 \quad (2)$$

where Q_a^{QL} is the energy flux of species a , and Γ^{QL} is the ambipolar particle flux calculated by the QL theory. Here $\Phi_{k_y}(\theta=0)$ is the maximum ($k_x=0$) normalized potential amplitude at the outboard midplane ($\theta=0$), $k_y = nq/r$ is the binormal mode number (q is the safety factor and r is the minor radius of the simulation), and ΔK_y is the interval between the mode numbers. c_{free} is a free calibration parameter chosen to fit QL fluxes to the calculated NL fluxes by the Eulerian δf -GK code CGYRO [22]. Here,

the QL weights $W Q_{k_y}^a$ and $W \Gamma_{k_y}$ are obtained from linear CGYRO calculation (linear GK) for each mode. Note that these weights are independent of Φ_{k_y} . To evaluate the QL fluxes in Eqs. (1) and (2) we use the Φ_{k_y} calculated by NL CGYRO. Comparisons of the QL fluxes and the NL fluxes from CGYRO are shown in Fig. 1. The NL simulations are electromagnetic ($\delta\phi$ and δA_{\parallel}), performed with kinetic electrons and ions, $T_e = T_i$, radial resolution $\max(k_x \rho_s) = 11$, and binormal toroidal resolution $\max(k_y \rho_s) = 1$. From the core to the edge, and at selected radial locations, CGYRO-calculated NL fluxes are shown in Fig. 1. The turbulence is predominantly electrostatic in the entire radial range with the peak of the flux distribution in the long-wavelength ion range $0.2 \lesssim k_y \rho_s \lesssim 0.4$. As an exercise for predicting the fluxes in the edge ($r/a \geq 0.9$), the calibration parameter c_{free} is first determined by matching the QL and NL CGYRO energy fluxes in the core ($r/a \leq 0.8$). Choosing c_{free} in this way, we observe that core QL fluxes accurately match NL CGYRO fluxes (within %10 uncertainty) as shown in Figs. 1(a) and 1(b) for the electron and ion heat flux, respectively. Strong agreement between QL and NL CGYRO in the core of L -mode plasma was recently reported [14], although QL breakdown in the plasma core has also been observed [19]. Moreover, electron energy flux Q_e is predicted accurately in the edge by the QL model. However, the fluxes of ion energy and particle, respectively Q_i and Γ , are significantly underpredicted in the edge by this QL model; that is, by a factor of 3 to 4. In what follows, we will examine the underlying assumptions that permit the application of QL theory.

Fundamental physics of QL transport.—Validity of QL theory is fundamentally determined at the microscopic level from particle dynamics. Particles are scattered by a complex evolving landscape of turbulent potential fields $\delta\phi$ and δA_{\parallel} . These fields have their own characteristic perpendicular and parallel length scale, λ_{\perp} and λ_{\parallel} , respectively, and timescale τ_c , which are obtained from the Eulerian correlation function. However, diffusive transport of particles and energy is determined by the step-size and correlation time of particle motion, not by those of the fields. For the scales associated with particle motion, the Lagrangian correlation function is evaluated. The timescale for particle motion is approximated by the flight time $\tau_{\text{FL}} = \mathcal{V}/\lambda_{\perp}$, where \mathcal{V} is a typical drift velocity for the particle. τ_{FL} describes the time needed for the particle to travel the entire span of the correlated region of length λ_{\perp} before leaving it for another correlated region. For a predominantly electrostatic turbulence the drift velocity is $\delta \mathbf{V}^E = c \mathbf{b} \times \nabla \delta\phi / B$, hence the drift velocity is proportional to $\delta\phi$ (c is the speed of light, B is the magnitude, and \mathbf{b} is the unit vector along the magnetic field). The Kubo number is defined as the ratio of these two timescales

$\mathcal{K} = \tau_c/\tau_{FL}$, and is a measure of the strength of turbulence and nonlinearity.

For QL theory to be valid, turbulence should be weak enough so that a particle cannot sample the whole correlated region it resides in before the landscape evolves [23,24]. This happens if the fields evolve and scatter the particle before it can drift across the correlated region ($\mathcal{K} < 1$). In this regime, particle motion is stochastic and the decorrelation is temporal (caused by the evolving landscape) with the random time step given by τ_c . These random spatial steps $\Delta \sim \mathcal{V}\tau_c$ result in perpendicular diffusion coefficient $D \sim \Delta^2/\tau_c = \mathcal{V}^2\tau_c$. This quadratic dependence on \mathcal{V} is characteristic of the quasilinear turbulence (QLT) scaling regime.

In stronger turbulence, a particle can quickly sample the correlated region before the landscape changes ($\mathcal{K} > 1$). In this case the particle is scattered due to the randomness of spatial structure of the potential landscape, not its temporal evolution. Therefore, the decorrelations of particle trajectories are spatial (with fixed landscape) with random step size $\Delta \sim \lambda_\perp$, i.e., the length of the correlated region. Hence, the random time step is given by τ_{FL} . The diffusion coefficient of this stochastic motion is given by $D \sim \Delta^2/\tau_{FL} = \mathcal{V}\lambda_\perp$. The linear dependence of D on \mathcal{V} is characteristic of the strong microturbulence (SMT) scaling regime. For macroscopic turbulence with $\Delta \sim a$, the latter regime becomes Bohm scaling, which requires a broader definition in transport theory [21,25–27].

Lagrangian calculation of transport.—Since CGYRO is an Eulerian code which self-consistently calculates the time-evolution of distribution functions and turbulence fields, the Lagrangian correlation which requires tracking of the particles cannot be simultaneously calculated. Hence, to obtain the Lagrangian correlation of turbulence, we developed a Lagrangian Gyrocenter Tracking code (LGT1). In this code, test particles are launched into the time-varying saturated turbulence, which is precalculated by CGYRO using direct gyrokinetic simulation. Lagrange’s equations of motion [28–31] adapted to the flux-tube configuration are solved in the field-aligned coordinates (r, θ, α) (radial, poloidal, and binormal) to obtain the test-particle gyrocenter orbits in 3D toroidal tokamak geometry identical to that in CGYRO. These particles experience the evolving turbulent field $\delta\phi$ (electrostatic). An initial distribution of particle energy is produced by a Maxwellian with average velocity given by the thermal velocity of the species V_{Ta} . The initial radial and binormal particle coordinates are randomly chosen inside the simulation box used by CGYRO. Also, the initial poloidal location is chosen randomly from the whole domain $[-\pi, \pi)$.

The Lagrangian correlation is calculated by tracing of the gyrocenters $L(t) = \langle \delta V_r^E(t) \delta V_r^E(0) \rangle$, where $\delta V_r^E = \delta \mathbf{V}^E \cdot \nabla r$, $\delta \mathbf{V}^E(t)$ is the $E \times B$ velocity of a particle along

its orbit at time t , and $\langle \dots \rangle$ denotes an ensemble average. We implicitly assume that the saturated turbulence is stationary in time, meaning that the Eulerian correlation of turbulent fields does not separately depend on two times t, t' but only on the difference $t - t'$. Practically, ensemble averaging is achieved by random launch positioning of gyrocenters within the initial 3D space and by time averaging along the particle orbits. To make sure the time averaging effectively captures the turbulence evolution, the turbulence fields used for the simulations evolve in a span of $T \sim \mathcal{O}(10 \tau_c)$. The Lagrangian diffusivity is then defined as $D_L = \int_0^\infty \bar{L}(t) dt$, where $\bar{L}(t) = \mathcal{F}[L(t)]$, $[\dots]$ denotes averaging over the particle energy distribution, and \mathcal{F} denotes averaging over the flux surface.

To verify LGT1 calculations of the gyrocenter motions, fluxes of particle and energy are calculated from the ensemble of test particles and compared to the fluxes correspondingly calculated by CGYRO. Importantly, we find that the LGT1-calculated fluxes are in good agreement with time-averaged CGYRO fluxes for both species (within roughly 20% uncertainty). We use LGT1 to determine the transport regime associated with the turbulence, i.e., QLT or SMT scaling, or something in between. To determine the scaling regime, we introduce a numerical scaling factor α_V such that $\delta\phi \rightarrow \alpha_V \delta\phi$. Scanning α_V above (below) unity will raise (lower) the potential peaks and make the troughs deeper (shallower). The particles experience the amplitude-modified potential, while the rate of turbulence evolution and τ_c stay the same. Hence, this test is essentially a systematic scan of nonlinearity strength, whereas the Kubo number’s timescale ratio is an approximate measure of nonlinearity strength based on dimensional arguments. For each scaling factor α_V the average drift velocity of particles is defined as $\bar{V}_r \equiv \sqrt{\bar{L}(0)} = \sqrt{\mathcal{F}[\langle (\delta V_r^E)^2 \rangle]}$. The log-log plot of the Lagrangian diffusion coefficient (D_L) in gyroBohm units versus \bar{V}_r in units of c_s/ρ^* for ions, shown in Fig. 2, is obtained by scanning α_V . Two radial regions are represented in two separate plots: the plasma core is represented at radius $r/a = 0.6$ in Fig. 2(a), and the plasma edge is represented at radius $r/a = 0.95$ in Fig. 2(b). The reference point for the scans where $\alpha_V = 1$ is shown with a white diamond symbol. In each plot two distinct branches are identified by their slope: the QLT branch and the SMT branch. The dashed straight (in log-log) lines are $Y = c(\bar{V}_r)^\kappa$ depicting the asymptotic slopes with scaling exponent κ at the extreme limits: $\kappa = 2$ for the QLT branch and $\kappa = 1$ for the SMT branch. The core turbulence shown in Fig. 2(a) is on the QLT branch. Therefore the QL theory is a valid approximation for this turbulence and the nonlinear fluxes depend approximately quadratically on \bar{V}_r (or equivalently on $\delta\phi$). This result is consistent with the region of agreement for the QL and NL fluxes observed in Fig. 1 in the plasma core. In contrast, edge turbulence ($r/a = 0.95$)

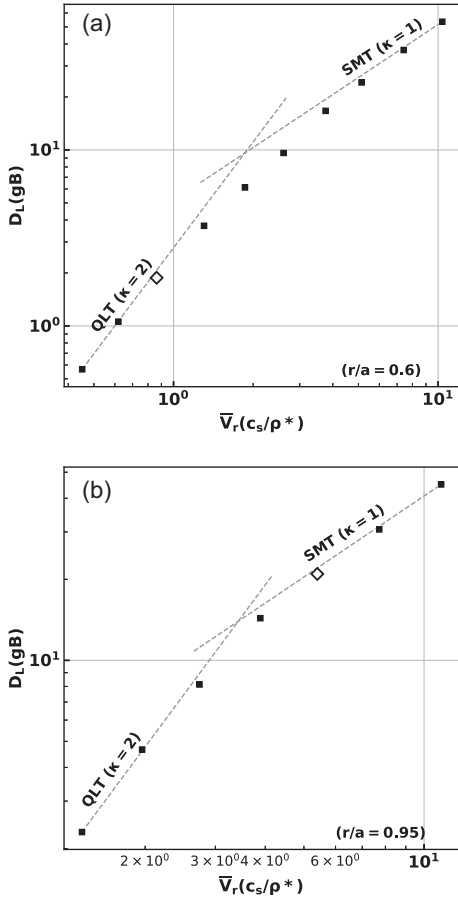


FIG. 2. Lagrangian diffusivity D_L versus average drift velocity \bar{V}_r for ions, for (a) core turbulence ($r/a = 0.6$) and (b) edge turbulence ($r/a = 0.95$). The reference point of the scan for which $\alpha_V = 1$ is shown with a white diamond symbol.

is clearly on the SMT branch, and consequently the QL theory is not a valid approximation.

We define a local scaling exponent,

$$\kappa_1 = \left. \frac{d \ln D_L}{d \ln \bar{V}_r} \right|_{\alpha_V=1}, \quad (3)$$

which measures the local slope determined from curves fitted to scans such as the ones in Fig. 2. For all the radial points in Fig. 1, κ_1 is evaluated and shown in Fig. 3(b). It can be seen that κ_1 decreases from the deep core to the edge. In the deep core ($r/a = 0.5, 0.6$), we find the turbulence to be on the QLT branch ($\kappa_1 \sim 1.7$). In the core-edge boundary, $0.7 \leq r/a \leq 0.8$, κ_1 has intermediate values $\kappa_1 \sim 1.5$, for which turbulence has departed from the QLT branch but is still not on the SMT branch. In the edge, $0.9 \leq r/a \leq 0.95$, turbulence is on the SMT branch of transport and $\kappa_1 \sim 1.1$. We also define a Kubo number using the calculated potential on the outboard midplane: $\mathcal{K} \equiv \mathcal{V} \tau_c / \lambda_{\perp,r}$, where $\mathcal{V} = c_s \sum_{n=1}^N (k_y \rho_s) \delta \hat{\phi}_{n,\text{rms}}(\theta = 0) / N$, and rms represents the root-mean-square time average of the potential

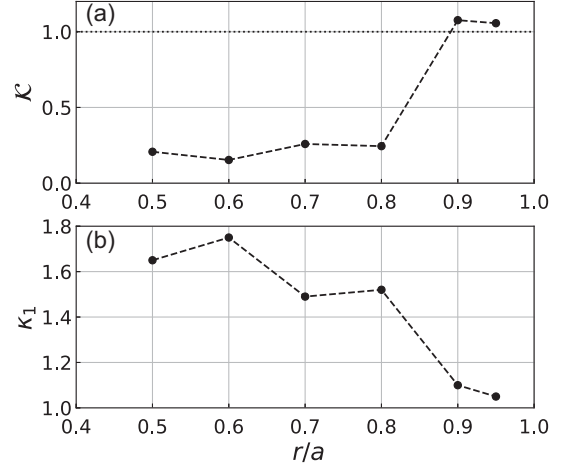


FIG. 3. (a) Kubo number \mathcal{K} and (b) scaling exponent κ_1 versus the normalized minor radius.

normalized to e/T_e . τ_c is determined by the characteristic width of the Eulerian autocorrelation function, and $\lambda_{\perp,r}$ is the equal-time radial correlation length calculated from the output of nonlinear CGRYO for the time averaged field. The evaluated \mathcal{K} shown in Fig. 3(a) increases from values below 1 in the core ($\mathcal{K} \lesssim 0.2$) to much larger values in the edge ($\mathcal{K} \sim 1$). This jump in \mathcal{K} implies that the nonlinearity strength increases in the edge beyond the validity of the QL approximation. This is consistent with the observed large under-prediction of Q_i and Γ by the QL model in Figs. 1(b) and 1(c). Comparing Figs. 3(a) and 3(b), it appears that the transition to the SMT regime happens for $\kappa_1 \sim 1.4$. However, a broader database study is needed to more accurately determine the QLT-to-SMT transition value for κ_1 .

Lagrangian analysis for electrons.—In order to perform a similar analysis for electrons, collisions must be included in the physics model. Especially in the edge region, which is much higher in collisionality, $\nu^* > 1$, effects of collisions are non-negligible for electrons. To recreate the test particle component of the Fokker-Planck collision operator employed in CGYRO [22,32] velocity changes are given to the particles in the event of collisions, which take place based on the Monte Carlo probability function $P = 1 - \exp(-\nu_a \Delta t)$ [33–35].

Performing the potential amplitude scan for electrons, analogous to those in Fig. 2, we find that electron turbulence is globally on the QLT branch, which is consistent with the good agreement between QL and NL Q_e fluxes over the entire radial range as shown in Fig. 1(a). This is especially interesting in the edge region ($r \geq 0.9$) for which we showed that ions are on the SMT branch of turbulence. This bifurcation in transport regime between the two species is essentially the result of small electron mass. We explore the electron transport regime in Fig. 4 for the edge ($r/a = 0.95$) which shows the potential amplitude scan of D_L for electrons in three different

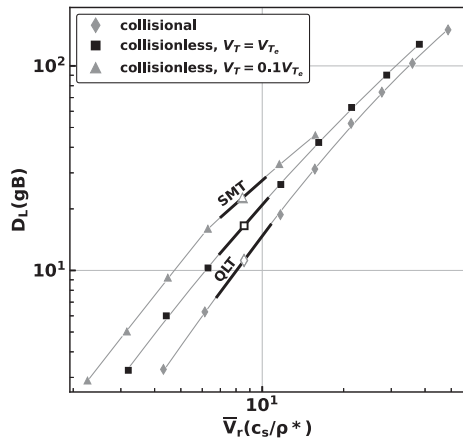


FIG. 4. Lagrangian diffusivity for electrons versus average drift velocity at $r/a = 0.95$. Decrease in the scaling exponent κ_1 (slope of solid lines) at the reference velocity of the scan (open symbols, $\alpha_V = 1$) shows the transition from the QLT to SMT branch of turbulence by going from collisional to slow-collisionless electrons.

settings: collisional, collisionless, and slow collisionless. Straight black lines show the local scaling exponent (slope κ_1) at the reference point of the scan ($\alpha_V = 1$) which is shown with open symbols. The gray curve interpolates each set of scan points with a test fitting function, shown for the purpose of better distinguishing the different scans. Diamond symbols show the scan for collisional electrons with the thermal velocity $v_{Te} \approx 61c_s$. Turbulence is on the QLT branch with local power $\kappa_1 = 1.77$. For the collisionless scan (square symbols) we set the collision rate to zero in LGT1. Here, we find that diffusivity has slightly departed from the QLT branch and the local exponent is reduced to $\kappa_1 = 1.53$. This departure shows that collisions have a decorrelating effect on the electron trajectories such that their paths are randomized by collisions before traversing their entire correlated regions, similar to the effect of turbulence evolution.

Because of their fast motion, electrons can escape the correlated region in the parallel direction before they traverse the whole perpendicular correlated region by the $E \times B$ drift. Therefore, the fast parallel motion also has a decorrelating effect for the particle orbits. Transport scaling in the absence of this parallel decorrelation is shown Fig. 4 (triangles) for the slow-collisionless scan: the electrons are again collisionless, moreover, they have been slowed down by reducing their thermal velocity $V_T = 0.1V_{Te}$. Reduced electron parallel velocity has eliminated the decorrelation effect that is present for the collisionless electrons at $V_T = V_{Te}$ (squares). We find that the slow-collisionless electrons (triangles) experience the turbulence on the SMT branch with local exponent $\kappa_1 = 1.15$.

So far QL models have been proven to be reasonably accurate and reliable for predicting the electrostatic turbulent transport in the tokamak core. However, there has

been limited progress in improving these models for the application to the complex region of the plasma edge. This situation is due in part to our lack of understanding of the complex nature of NL physics of turbulence. Breaking of the validity of QL theory, as demonstrated in this Letter, indicates that prediction of transport in the plasma edge requires more advanced physics-based models, beyond the strictly QL models. Specifically, by characterizing the dependence of transport on the turbulence strength, advanced models should be able to capture the transition of ion transport to the SMT regime. This work provides the necessary understanding and quantitative tools for developing such predictive transport models that go beyond the QL theory.

The first author (A. A.) wishes to thank R. E. Waltz for his encouragement and valuable discussions. This work was supported by US DOE under Grants No. DE-FC02-06ER54873 and No. DE-FG02-95ER54309.

This report was prepared as an account of work sponsored by an agency of the U.S. Government. Neither the U.S. Government nor any agency thereof, nor any of their employees, makes any warranty, express or implied for the accuracy, completeness, or usefulness of any information, apparatus, product, or process disclosed, or represents that its use would not infringe privately owned rights. Reference herein to any specific commercial product, process, or service by trade name, trademark, manufacturer, or otherwise does not necessarily constitute or imply its endorsement, recommendation, or favoring by the U.S. Government or any agency thereof. The views and opinions of authors expressed herein do not necessarily state or reflect those of the U.S. Government or any agency thereof.

*ashourvana@fusion.gat.com

- [1] R. J. Groebner, K. H. Burrell, and R. P. Seraydarian, *Phys. Rev. Lett.* **64**, 3015 (1990).
- [2] P. Gohil, T. C. Jernigan, T. H. Osborne, J. T. Scoville, and E. J. Strait, *Nucl. Fusion* **50**, 064011 (2010).
- [3] J. Menard, B. Grierson, T. Brown, C. Rana, Y. Zhai, F. Poli, R. Maingi, W. Guttenfelder, and P. Snyder, *Nucl. Fusion* **62**, 036026 (2022).
- [4] D. B. Weisberg *et al.*, *Fusion Sci. Technol.* **79**, 320 (2023).
- [5] P. Rodriguez-Fernandez, A. Creely, M. Greenwald, D. Brunner, S. Ballinger, C. Chrobak, D. Garnier, R. Granetz, Z. Hartwig, and N. Howard, *Nucl. Fusion* **62**, 042003 (2022).
- [6] P. Schneider *et al.*, *Nucl. Fusion* **62**, 026014 (2022).
- [7] C. Chrystal, B. Grierson, S. Haskey, A. Sontag, F. Poli, M. Shafer, and J. deGrassie, *Nucl. Fusion* **60**, 036003 (2022).
- [8] J. Weiland, *Stability and Transport in Magnetic Confinement Systems* (Springer, New York, 2012).
- [9] H. Biglari, P. H. Diamond, and P. W. Terry, *Phys. Fluids B: Plasma Phys.* **2**, 1 (1990).

- [10] G. M. Staebler, R. E. Waltz, J. Candy, and J. E. Kinsey, *Phys. Rev. Lett.* **110**, 055003 (2013).
- [11] G. M. Staebler, J. Candy, N. T. Howard, and C. Holland, *Phys. Plasmas* **23**, 062518 (2016).
- [12] G. M. Staebler, E. A. Belli, J. Candy, J. E. Kinsey, H. Dudding, and B. Patel, *Plasma Phys. Contr. Fusion* **61**, 116007 (2021).
- [13] J. Citrin, C. Bourdelle, F. J. Casson, C. Angioni, N. Bonanomi, Y. Camenen, X. Garbet, L. Garzotti, T. Görler, O. Gürcan, F. Koechl, F. Imbeaux, O. Linder, K. van de Plassche, P. Strand, G. Szepesi, and J. Contributors, *Plasma Phys. Contr. Fusion* **59**, 124005 (2017).
- [14] G. M. Staebler, J. Candy, E. A. Belli, J. E. Kinsey, N. Bonanomi, and B. Patel, *Plasma Phys. Contr. Fusion* **63**, 015013 (2021).
- [15] C. Bourdelle, X. Garbet, F. Imbeaux, A. Casati, N. Dubuit, R. Guirlet, and T. Parisot, *Phys. Plasmas* **14**, 112501 (2007).
- [16] R. E. Waltz, A. Casati, and G. M. Staebler, *Phys. Plasmas* **16**, 072303 (2009).
- [17] J. Candy and R. Waltz, *J. Comput. Phys.* **186**, 545 (2003).
- [18] V. Grandgirard, J. Abiteboul, J. Bigot, T. Cartier-Michaud, N. Crouseilles, G. Dif-Pradalier, C. Ehrlacher, D. Esteve, X. Garbet, P. Ghendrih, G. Latu, M. Mehrenberger, C. Nordsieck, C. Passeron, F. Rozar, Y. Sarazin, E. Sonnendrücker, A. Strugarek, and D. Zarzoso, *Comput. Phys. Commun.* **207**, 35 (2016).
- [19] C. Gillot, G. Dif-Pradalier, Y. Sarazin, C. Bourdelle, A. B. Navarro, Y. Camenen, J. Citrin, A. D. Siena, X. Garbet, P. Ghendrih, V. Grandgirard, P. Manas, and F. Widmer, *Plasma Phys. Contr. Fusion* **65**, 055012 (2023).
- [20] Correlated range is the scale describing the width the equal-time Eulerian correlation function, beyond which the correlation function is small.
- [21] R. Balescu, *Aspects of Anomalous Transport in Plasmas* (Institute of Physics Publishing, Bristol and Philadelphia, 2005), Chap. 6,14.
- [22] J. Candy, E. Belli, and R. Bravenec, *J. Comp. Physiol.* **324**, 73 (2016).
- [23] J. Misguich, J. Reuss, M. Vlad, and F. Spineanu, *Physica Mag.* **20**, 103 (1998).
- [24] M. Ottaviani, *Physica Mag.* **20**, 95 (1998).
- [25] T. Dupree, *Phys. Fluids* **10**, 1049 (1968).
- [26] R. E. Waltz, J. C. DeBoo, and M. N. Rosenbluth, *Phys. Rev. Lett.* **65**, 2390 (1990).
- [27] J. M. Dawson, H. Okuda, and R. N. Carlile, *Phys. Rev. Lett.* **27**, 491 (1971).
- [28] R. G. Littlejohn, *Phys. Fluids* **28**, 2015 (1985).
- [29] T. S. Hahn, *Phys. Fluids* **31**, 2670 (1988).
- [30] S. Ku, C. S. Chang, R. Hager, R. M. Churchill, G. R. Tynan, I. Cziegler, M. Greenwald, J. Hughes, S. E. Parker, M. F. Adams, E. D’Azevedo, and P. Worley, *Phys. Plasmas* **25**, 056107 (2018).
- [31] R. Hager, C. S. Chang, N. M. Ferraro, and R. Nazikian, *Phys. Plasmas* **27**, 062301 (2020).
- [32] E. Belli and J. Candy, *Plasma Phys. Contr. Fusion* **54**, 015015 (2012).
- [33] C. Birdsall, *IEEE Trans. Plasma Sci.* **19**, 65 (1991).
- [34] P. Helander and D. J. Sigmar, *Collisional Transport in Magnetized Plasmas* (Cambridge University Press, Cambridge, 2002), Chap. 3, p. 35.
- [35] E. A. Belli and J. Candy, *Plasma Phys. Contr. Fusion* **54**, 015015 (2012).